Charge exchange and dissociative processes in collisions of slow He²⁺ ions with H₂O molecules

B. Seredyuk, R. W. McCullough, H. Tawara, and H. B. Gilbody
Queen's University Belfast, Belfast BT7 1NN, United Kingdom

D. Bodewits and R. Hoekstra
KVI Atomic Physics, Zernikelaan 25, NL 9747 AA Groningen, The Netherlands

A. G. G. M. Tielens
Kapteyn Institute/SRON, PO Box 800, 9700 AV Groningen, The Netherlands

P. Sobocinski, D. Pesic, R. Hellhammer, B. Sulik,* and N. Stolterfoht
Hahn-Meitner Institut Berlin, Glienickerstraβe 100, D-14109 Berlin, Germany

O. Abu-Haija and E. Y. Kamber
Department of Physics, Western Michigan University, Kalamazoo, Michigan 49008-5252, USA
(Received 1 November 2004; published 10 February 2005)

Experimental and theoretical studies of one-electron capture in collisions of He²⁺ ions with H₂O molecules have been carried out in the range 0.025–12 keV amu⁻¹ corresponding to typical solar wind velocities of 70–1523 km s⁻¹. Translational energy spectroscopy (TES), photon emission spectroscopy (PES), and fragment ion spectroscopy were employed to identify and quantify the collision mechanisms involved. Cross sections for selective single electron capture into $n=1$, 2, and 3 states of the He⁺ ion were obtained using TES while PES provided cross sections for capture into the He⁺(2p) and He⁺(3p) states. Our model calculations show that He⁺($n=2$) and He⁺($n=3$) formation proceeds via a single-electron process governed by the nucleus-electron interaction. In contrast, the He⁺(1s) formation mechanism involves an exothermic two-electron process driven by the electron-electron interaction, where the potential energy released by the electron capture is used to remove a second electron thereby resulting in fragmentation of the H₂O molecule. This process is found to become increasingly important as the collision energy decreases. The experimental cross sections are found to be in reasonable agreement with cross sections calculated using the Demkov and Landau-Zener models.

I. INTRODUCTION

Cometary X-Ray and far-ultraviolet emissions are produced when multiply charged ions in the solar wind collide with neutral particles in the coma [1]. The resulting charge exchange spectra can be used to probe solar wind properties such as the velocity, density, and composition as shown previously [2–4]. To make full use of the diagnostic qualities of comets as solar wind probes, experimental data on typical comet-solar wind collision systems are essential. Although some experimental and theoretical work exists, many major data gaps still need to be bridged [5]. One of the most striking gaps is the lack of knowledge on the interaction of alpha particles with water vapor.

When comets approach the Sun, near-surface ice starts to sublimate and large clouds of gas are formed around the comet, the nucleus of which produces mainly water vapor. The spatial extent of the molecular cloud formed is determined primarily by the solar radiation field. H₂O and OH have very short lifetimes compared with CO, H, and O so that, whereas the inner regions of the coma consist mainly of water vapor, the outer regions are populated with its disso-

ciation products. The density distribution of cometary water molecules is thus closely linked to the heliocentric distance of the comet. The probability of a solar wind ion reaching the water vapor dominated region depends on the sublimation rate from the comet and the electron capture cross section of the ion involved. In practice, water vapor plays a major role in almost all of scenarios where solar wind helium ions interact with cometary atmospheres.

An understanding of the interaction of alpha particles with H₂O molecules is also directly relevant to a detailed understanding of radiation damage in biological systems. The induction of DNA single and double strand breaks is to a large extent due to the action of secondary particles formed in the primary track induced by either alpha, beta, or gamma radiation. Since water is the natural environment of DNA, data for fragmentation and ionization of water molecules by alpha particles is an important prerequisite for building microscopic models.

In this paper we present, a comprehensive set of experimental data and theoretical predictions for state selective one-electron capture by He²⁺ ions in H₂O at velocities typical for the solar wind (70–1523 km s⁻¹ or ~0.025–12 keV amu⁻¹). The experimental data have been obtained in four independent laboratories using the experimental techniques of translational energy spectrometry (TES), photon emission spectroscopy (PES), and fragment

---

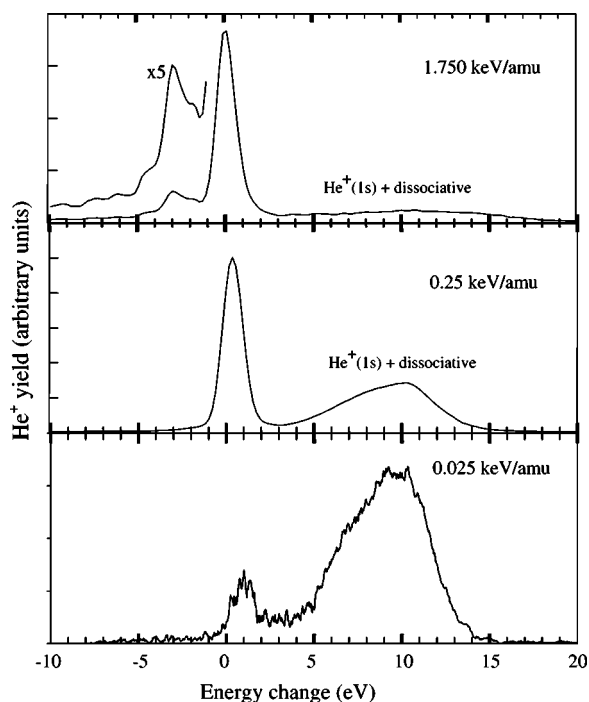*Permanent address: MTA ATOMKI, H-4001 Debrecen, Hungary.

FIG. 1. Energy change spectra for one electron capture by He^{2+} ions in H_2O at three representative energies recorded by the QUB and WMU translational energy spectrometers (see text).
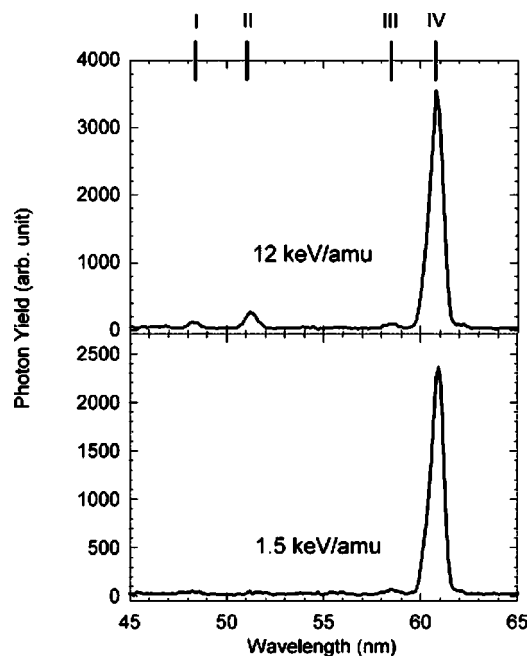

FIG. 2. Photon emission spectra for one-electron capture in $He^{2+}-H_2O$ collisions observed at two different velocities. The following emission features are indicated: I—second order of He II $(4p$-$1s)$ at 24.3 nm; II—second order of He II $(3p$-$1s)$ at 25.6 nm; III—He I $(1s2p$-$1s^2)$ at 58.4 nm; IV—second order of He II $(2p$-$1s)$ at 30.4 nm.

ion spectrometry (FIS). Previously, only total electron capture cross sections were available [6–8] and these have been combined to provide a set of recommended cross sections for both one- and two-electron capture in the energy range 0.05–5.19 keV amu^{-1} [9]. Measurements of state selective single electron capture processes for the $He^{2+}-H_2O$ system were carried out by Abu-Haija *et al.* [10], using translational energy spectrometry (TES) in the range of 25 to 375 eV amu^{-1}. Dissociative transfer ionization (DTI) was found to become more important than nondissociative processes as the impact energy was decreased.

TABLE I. Product channels and corresponding energy defects for one-electron capture by He^{2+} ions in H_2O.

Product channels	Energy defects (eV)
He^+ $(n=3)+H_2O^+[\widetilde{A}^2A_1]$	-7.79–-10.61
He^+ $(n=3)+H_2O^+[\widetilde{X}^2B_1]$	-6.57–-7.35
He^+ $(n=2)+H_2O^+[\widetilde{B}^2B_2]\Rightarrow OH^+,O^+,H^+$	-4.50–-5.11
He^+ $(n=3)+H_2O^+[\widetilde{B}^2B_2]$	-3.57–-6.39
He^+ $(n=2)+H_2O^+[\widetilde{A}^2A_1]$	-0.23–-3.05
He^+ $(n=2)+H_2O^+[\widetilde{X}^2B_1]$	0.20–0.98
He^+ $(n=1)+H_2O^{2+}[^3B_1]+e$	17.90
He^+ $(n=1)+H_2O^{2+}[^1A,^1B]+e$	12.40–14.40
He^+ $(n=1)+H_2O^{2+}[(2)^1A_1]+e$	9.10

II. EXPERIMENTAL METHODOLOGY

A. Translational energy spectrometry (TES)

Two TES spectrometers were employed in this work. At Queen's University, Belfast (QUB) measurements were carried out in the energy range 250–2000 eV amu^{-1} while at Western Michigan University (WMU) measurements were carried out in the energy range 25–375 eV amu^{-1}. In the QUB measurements, He^{2+} ions were produced by an ECR ion source while the WMU experiment employed a recoil ion source. Full details of these spectrometers and measurement procedure have been given in previous publications [11,12] and references therein. Only a brief summary of the main features need be given here.

The TES measurements rely on careful measurements of the difference ΔT between the kinetic energy of the He^{2+} primary ion and the fast forward-scattered He^+ product ion. The identification and determination of the relative importance of the collision product channels characterized by energy defects ΔE was carried out with an energy resolution of 1 eV (full width at half maximum). The angular acceptance of the product ion energy analyzer was $\pm 3°$ for the QUB measurements and $\pm 8°$ for the WMU measurements.

Figure 1 shows three representative energy change spectra from the QUB and WMU translational energy spectrometers. Analysis of the position and magnitude of the peaks in the observed energy change spectra enables identification and determination of the relative contribution of each product channel. Table I lists the possible collision product channels with energy defects which correlate with the observed peaks
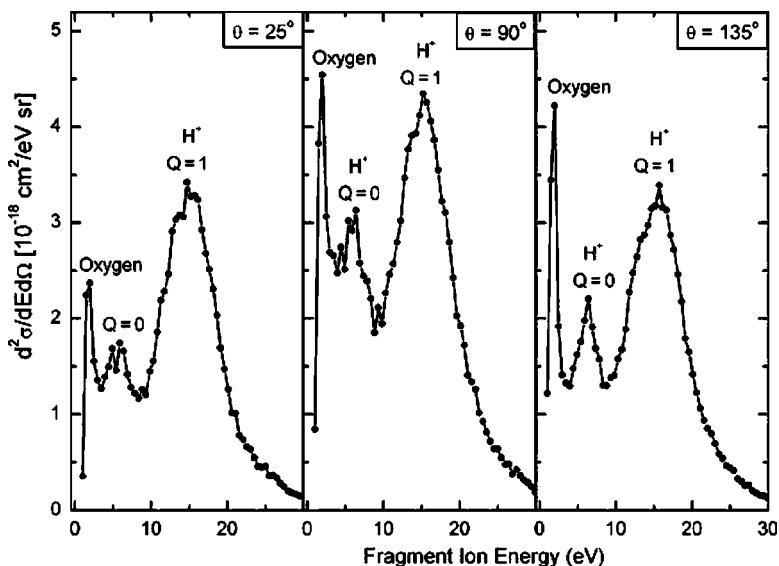
FIG. 3. Energy spectra of fragment ions from the interaction of 4-kev He^{2+} ions with H_2O molecules. The observed fragments are formed exclusively in large impact parameter collisions. The observation angles were $\Theta = 25°$, 90°, and 135°.

in the energy change spectra for one-electron capture by He^{2+} ions in H_2O. Energy levels for the relevant H_2O^+ states and their associated vibrational energy distributions were obtained from photoelectron spectroscopy measurements [13] and, for the H_2O^{++} states, from the photo ion–photo ion coincidence measurements of Richardson [14]. The He^+ energy levels were obtained from the tabulations of Bashkin and Stoner [15]. The sum of the relative yields of the individual capture processes resulting in He^+ ($n=1$), He^+ ($n=2$), and He^+ ($n=3$) formation, identified in the QUB energy change spectra, were normalized to the recommended total one-electron capture cross sections of Greenwood *et al.* [9]. The WMU data for He^+ ($n=1$) and He^+ ($n=2$) formation were determined from absolute measurements of the target pressures and detector efficiencies.

B. Photon emission spectroscopy (PES)

In the photon emission spectroscopy (PES) experiment at the KVI, a He^{2+} ion beam, extracted from an ECR ion source, with energies between 1.5 and 12 keV amu^{-1} was crossed with a neutral gas jet (see Ref. [16]. A VUV spectrometer (5–80 nm) was used to record the emission spectra following charge exchange. Absolute wavelength and sensitivity calibration of the VUV system was achieved by cross referencing previous measurements on systems with well established cross sections (see Ref. [17]). The spectrometer is equipped with a position sensitive detector allowing for the simultaneous detection of a wavelength window of approximately 20 nm.

Two representative spectra for collisions between He^{2+} and water vapor are shown in Fig. 2. Note that the He II Lyman series is observed in second order, therefore the He II $(2p-1s)$, He II $(3p-1s)$ appear at 60.4 and 51.2 nm, respectively. Emission from higher $He^{1+}(np)$ states is detected (around 48 nm). At 58.4 nm, the He I $(1s2p-1s^2)$ transition is observed which results from simultaneous a two-electron capture process. The spectra are clearly dominated by the He II $(2p-1s)$ line emission.
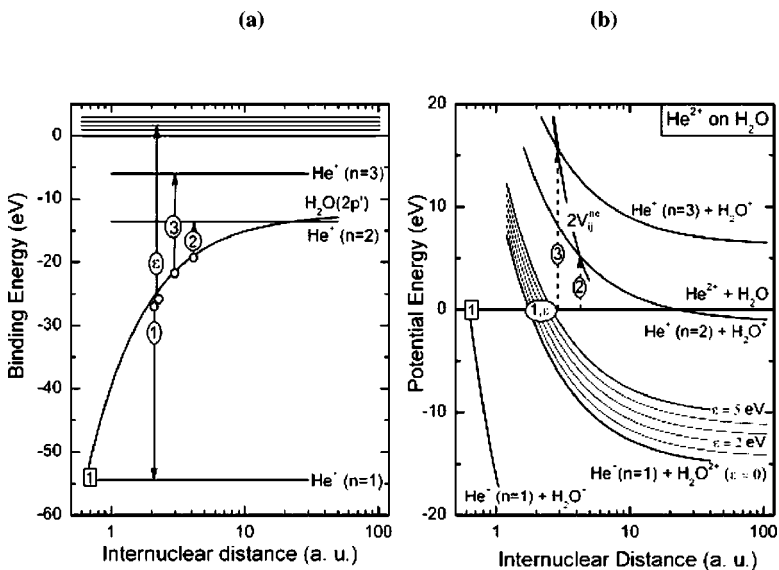
(a)   (b)

FIG. 4. (a) Correlation diagrams of molecular orbitals and (b) corresponding potential curves for the He^{2+}-H_2O system. Single-electron transitions populating the $n=1$, 2, and 3 states of He^+ are denoted by 1, 2, and 3, respectively. Dielectronic transitions populating the $n=1$ state and the continuum state ε are denoted $(1,\varepsilon)$.
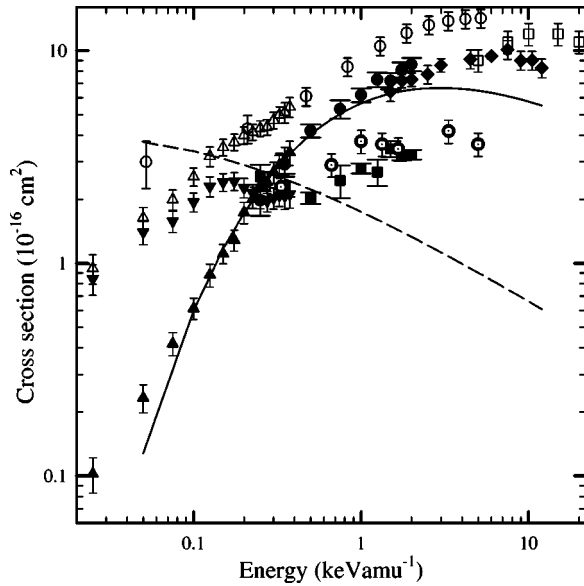
FIG. 5. Cross sections for one electron capture by He^{2+} ions in H_2O. Total cross sections: open squares, Rudd *et al.* [6]; open circles, Greenwood *et al.* [9]; open triangles, present work. Capture into He^+ ($n=2$) states: closed circles, QUB; closed triangles, WMU. He II ($2p$-$1s$): closed diamonds, KVI. Capture into He^+ ($n=1$) state: closed squares, QUB; inverted triangles, WMU. Transfer ionization: circles with cross hairs, HMI. Theory: solid line, He^+ ($n=2$) formation; dashed line, He^+ ($n=1$) formation.
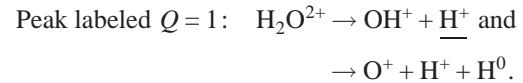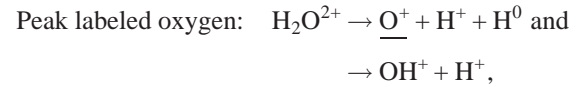
C. Fragment ion spectroscopy (FIS)

The fragment ion spectrometer (FIS) at HMI has been described by Pešić *et al.* [18] so that only a short description will be given here. He^{2+} ions in the energy range 0.25–5 keV amu^{-1} were produced by a 14.5-GHz ECR ion source. The experimental chamber contains an electrostatic parallel-plate spectrometer with a relative energy resolution of 5% and an angular resolution of 4°. The spectrometer was rotated from 18° to 135° with respect to the incident ion-beam direction. The absolute efficiency of the spectrometer was calibrated by reproducing data from previous measurements [18] where a detailed description of the normalization procedure to determine absolute cross sections has also been reported.

The spectra of ions measured using the FIS method contain dominant peaks in the energy range from 0 to about 30 eV as shown in Fig. 3. The spectral structures are associated with Coulomb explosion (CE) mechanisms after removal of two electrons from the H_2O molecule. The kinetic energy distribution of the detected ions is interpreted within a scenario where two or more electrons from the molecule are suddenly removed by the incident ion so that the molecule becomes unstable and dissociates into charged and/or neutral particles. Then, knowing the initial separations of the atoms in the H_2O molecule and treating the ions as point charges, one can calculate the kinetic energies of the fragments. Thus the following fragmentation channels are identified and the observed fragments from each channel that contribute to the peaks in Fig. 3 are underlined:

TABLE II. Absolute cross sections for transfer ionization (TI) in He^{2+}-H_2O collisions obtained by subtracting cross sections for double capture (DC) from our measured sum (TI+DC) as detailed in the text. Cross sections DC are interplated values from the data of Greenwood *et al.* [9].

Energy (keV amu^{-1})	TI+DC (10–16cm2)	DC (10^{-16}cm^2)	TI (10^{-16}cm^2)
0.33	7.89	5.60	2.29
0.67	7.01	4.11	2.90
1.00	7.26	3.51	3.75
1.33	6.81	3.18	3.63
1.67	6.48	3.03	3.45
3.33	7.08	2.89	4.19
5.00	6.48	2.80	3.63
6.67	6.70		

Peak labeled oxygen: $H_2O^{2+} \rightarrow \underline{O^+} + H^+ + H^0$ and

$$\rightarrow \underline{OH^+} + H^+,$$

Peak labeled $Q=0$: $H_2O^{2+} \rightarrow O^0 + \underline{H^+} + H^+,$

Peak labeled $Q=1$: $H_2O^{2+} \rightarrow OH^+ + \underline{H^+}$ and

$$\rightarrow O^+ + H^+ + H^0.$$

Note that the peak labeled oxygen is formed by the slow fragment ions O^+ and OH^+, while the other peaks are formed by H^+. With the present experimental technique we cannot separate the fragments O^+ and OH^+, both of which contribute to peaks labeled oxygen. Due to their relatively small energy, we expect a low detection efficiency for O^+ and OH^+ ions so they will not be considered further.

In Fig. 3 the FIS spectra are plotted for the observation angles 25°, 90°, and 135°. The observed structures are rather similar while the overall intensity is found to be anisotropic with a spectral enhancement in the angular range from 70° to 90°. To obtain total cross sections for the production of H^+ fragments, the experimental data were integrated over the energy range from 3 to 35 eV (excluding the oxygen peak) and, subsequently, over the emission angle. Our measured cross sections are determined by mechanisms involving the removal of two electrons from the H_2O molecule through transfer ionization (TI) and double capture (DC):

$$He^{2+} + H_2O \rightarrow He^0 + H_2O^{2+} \text{ (DC)} \rightarrow He^+ + H_2O^{2+} + e \text{ (TI)}.$$

To obtain cross sections for TI, leading to He^+ ($n=1$) formation, the DC cross sections measured previously by Greenwood *et al.* [9] have been subtracted from the present results for the cross section sum TI+DC. The TI cross sections obtained in this way are shown in Table II and plotted in Fig. 5. Uncertainties in the TI data are estimated to be $\pm25\%$.

III. THEORETICAL DESCRIPTION

In the theoretical treatment we consider two types of capture mechanisms. First, transitions between quasiparallel po-

TABLE III. Cross sections (in units of 10^{-16} cm^2) for one-electron capture by He^{2+} ions in H$_2$O leading to He$^+$ ($n=1$), He$^+$ ($n=2$,) and He$^+$ ($n=3$) formation measured using the TES and PES techniques.

Energy (keV/amu)	TES ($n=1$) (WMU)	TES ($n=2$) (WMU)	TES ($n=1$) (QUB)	TES ($n=2$) (QUB)	PES ($2p$-$1s$) (KVI)	TES ($n=3$) (QUB)	PES ($3p$-$1s$) (KVI)
0.025	0.84±0.13	0.10±0.01					
0.050	1.40±0.17	0.23±0.03					
0.075	1.57±0.18	0.41±0.05					
0.100	1.94±0.19	0.61±0.07					
0.125	2.30±0.24	0.88±0.10					
0.150	2.40±0.23	1.11±0.11					
0.175	2.42±0.23	1.28±0.14					
0.200	2.26±0.23	1.73±0.19					
0.225	2.14±0.20	2.00±0.19					
0.250	1.99±0.19	2.31±0.23	2.56±0.35	1.98±0.31		0.04±0.01	
0.275	1.96±0.21	2.41±0.27					
0.300	2.02±0.23	2.67±0.30					
0.325	2.08±0.24	2.90±0.38					
0.350	2.07±0.28	3.05±0.45	2.30±0.25	2.92±0.29		0.05±0.01	
0.375	2.11±0.29	3.31±0.43					
0.500			2.03±0.13	4.20±0.30		0.06±0.01	
0.750			2.45±0.43	5.32±0.53		0.12±0.05	
1.000			2.80±0.16	6.18±0.45		0.19±0.04	
1.250			2.69±0.38	7.32±0.58		0.21±0.14	
1.500			3.45±0.31	7.22±0.64	6.43±0.65	0.39±0.15	0.04±0.01
1.750			3.19±0.13	8.15±0.67	7.22±0.52	0.43±0.26	0.07±0.01
2.000			3.24±0.17	8.62±0.62	7.32±0.53	0.46±0.02	0.07±0.01
2.500					7.75±0.78		0.07±0.01
3.000					8.54±0.61		0.10±0.01
4.500					9.12±0.92		0.14±0.02
6.000					9.43±0.28		0.18±0.01
7.500					10.12±1.02		0.29±0.03
9.000					8.99±0.91		0.29±0.04
10.50					9.01±0.91		0.39±0.05
12.00					8.30±0.84		0.50±0.06

tential curves, treated by the model developed by Demkov [19] and second, transitions at curve crossings, treated by the Landau [20]–Zener [21] model. The capture mechanisms are visualized using correlation diagrams of molecular orbitals and corresponding potential curves shown in Figs. 4(a) and 4(b), respectively. The MO diagram in Fig. 4(a) is useful to visualize the different capture mechanisms whereas Fig. 4(b) shows the transition energies involved. The transitions into the $n=2$ states of He$^+$ occur at distances near 4 a.u. (see the arrow labeled 2) initiated by the mechanisms considered by Demkov [19]. Similarly, Demkov-type transitions into the $n=3$ level of He$^+$ occur at about 3 a.u. (arrow labeled 3). In Fig. 4(b), the Demkov transitions occur at locations where the potential-energy difference is equal to twice the interaction matrix element V_{ij}^{ne}.

Population of the $n=1$ level of He$^+$ occurs near 2 a.u. as a result of a two-electron (dielectronic) process in which one electron is transferred into the MO correlated with the $n=1$ level and another electron is ionized. This transfer ionization (TI) process is produced by an electron-electron interaction, where the potential energy, liberated by the transition into the deeply lying $n=1$ orbital, is used to emit another electron (the sum of potential energies is equal to zero). In Fig. 4(b), the dielectronic transitions, denoted $(1, \varepsilon)$, occur at the locations where the incident channel He^{2+}+H$_2$O crosses a series of potential curves He$^+$+H$_2$O$^{2+}(\varepsilon)$. This results in the transfer of one electron of H$_2$O to the He^{2+} ion while a second electron is transferred into the continuum of H$_2$O with an energy ε.

Since the models of Demkov and Landau and Zener have been extensively treated in the literature by Salop and Olson [22] and by Stolterfoht [23] the theoretical method will only be briefly described here. Within the Demkov model the transition probability from the initial and final state is given by

$$p_D = \exp\left(-\frac{\Delta E_c}{\alpha v_p}\right), \tag{1}$$

where ΔE_c is the energy difference between the potential curves involved and v_p is the radial velocity of the projectile. The velocity parameter $\alpha = (\sqrt{2I_i} + \sqrt{2I_f})/2$ is obtained from the binding energies I_i and I_f of the electron in the initial and final state, respectively. Since the transition region is passed twice in a collision, the double passage probability is evaluated using the well-known statistical rule of Salop and Olson [22], $P_{if} = 2p_D(1-p_D)$.

We recall that the transitions considered here take place at a specific distance R_c so that one may use a "geometric" expression for the cross section,

$$\sigma_{if} = P_{if}(R_c)\pi R_c^2 \tag{2}$$

which implies that $P_{if}(R) = P_{if}(R_c) = \text{const}$ for $R < R_c$ and $P_{if}(R) = 0$ elsewhere.

The Landau-Zener (LZ) model treats transitions at crossings of diabatic states at distance R_c. In Fig. 4(b) the region of crossings of the initial states $He^{2+} + H_2O$ with various (continuum) states $He^+ (n=1) + H_2O^{2+} (\varepsilon)$ is labeled $(1, \varepsilon)$. The LZ model evaluates the probability p_{LZ} to remain in the initial diabatic state in a single crossing,

$$p_{LZ} = \exp\left(-\frac{2\pi H_c^2}{F_c v_p}\right), \tag{3}$$

where the "force" F_c is obtained as the derivative of the energy difference ΔE at R_c. The dielectronic matrix element $H_c = H_{ij}^{ee}(R_c)$ is evaluated at R_c and v_p is the projectile velocity, as before. For dielectronic transitions, produced by the electron-electron (*ee*) interaction, the matrix element may be approximated by

$$H_{if}^{ee} = 0.15\alpha^2 \exp(-0.86\alpha R)$$

[24], where α is the velocity parameter already given in conjunction with the Demkov theory.

For $p_{LZ} \ll 1$ the probability for populating the number v of final states is obtained as $P_{if} = 1 - p_{LZ}^{2v}$. The unknown number of final states was set to be equal to $v = 20$. For such a large number the results do not change significantly with increasing v. Therefore the choice of v is uncritical for the transition probability. It should be noted that the dielectronic matrix elements H_{ij}^{ee} are relatively small in comparison with the matrix elements V_{ij}^{ne} responsible for Demkov-type transitions. However, this smallness is compensated by the relative high number v of final states. After the transition probability is evaluated, the corresponding cross section is again obtained using Eq. (2).

IV. RESULTS AND DISCUSSION

The TES measurements, as illustrated by the three representative spectra shown in Fig. 1, enable the relative importance of the various one-electron capture channels to be determined. The two main features evident in these spectra are sharp peaks in the energy change region below 3 eV and a broader peak in the region of 4–17 eV. The peaks below 3
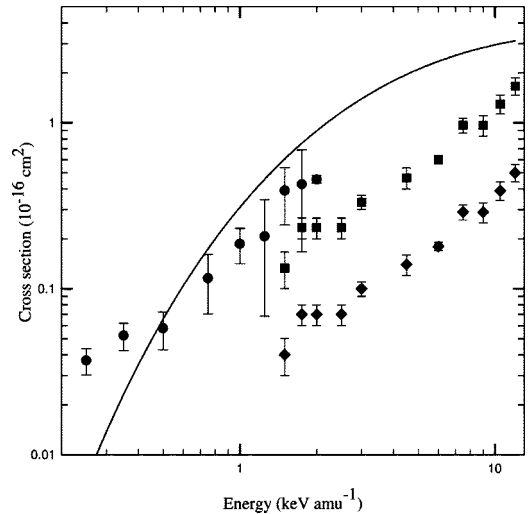

FIG. 6. Cross sections for He^+ ($n=3$) formation through one-electron capture in He^{2+}-H_2O collisions. Closed circles, TES data; closed diamonds, measured He^+ ($3p$-$1s$) photon emission cross sections; closed squares He^+ ($n=3$) formation cross sections from PES measurements assuming a statistical distribution of capture into He^+ ($3s$, $3p$, and $3d$) states; solid line, our calculated He^+ ($n=3$) formation cross sections.

eV can be correlated with He^+ ($n=2$) + H_2O^+ and He^+ ($n=3$) + H_2O^+ product channels (see Table I). The broad distribution above 4 eV corresponds to He^+ ($n=1$) formation with H_2O formed in doubly charged states via an Auger-type process (see Ref. [14]). These doubly charged states are unstable and subsequently dissociate. Cross sections for the formation of He^+ ($n=1$, 2, and 3) states at energies above 0.025 eV amu^{-1} have been determined by normalizing the integrated TES energy change spectra at each energy to the recommended total one-electron capture cross sections of Greenwood *et al.* [9]. As stated earlier, for energies below 0.25 eV amu^{-1}, the TES measurements by the WMU group were obtained by absolute calibration of the target gas pressure and detector efficiencies.

In Fig. 5 the measured cross sections for selective capture into the He^+ ($n=1$) and He^+ ($n=2$) states through the channels listed in Table I are compared with the corresponding results of the model calculations described above. These cross sections are also tabulated in Table III. Since capture into the $n=3$ levels of He^+ is insignificant compared with $n=1$ and $n=2$, we have also shown the sum of He^+ ($n=1$) and He^+ ($n=2$) formation cross sections for comparison with the recommended total cross sections of Greenwood *et al.* [9]. The agreement is excellent in the energy region of overlap. However, at energies below 0.2 keV amu^{-1} our measurements are seen to fall below the Greenwood *et al.* [9] data. In the energy region of overlap, the ratio between the PES data for He II ($2p$-$1s$) and the TES results for He^+ ($n=2$) formation is in accord with a statistical distribution. The He^+ ($n=1$) formation channels were observed using the TES and FIS techniques. There is good agreement between the TES results from QUB and WMU in the energy range of overlap and also with the He^+ ($n=1$) formation data derived from the FIS measurements.

4Cross sections for He$^+$ ($n=3$) formation measured using TES and our calculated values are shown in Fig. 6. We also include He$^+$ ($n=3$) formation cross sections derived from our PES measurements of the He$^+$ ($3p-1s$) emission cross sections by assuming a statistical distribution over the angular momenta. The agreement between the TES and PES data in the energy region of overlap is not unreasonable. In addition, despite the simplicity of the theoretical models used there is good general accord between experiment and theory. The probabilities for one-electron capture into the He$^+$ ($n=2$ and 3) states predicted by the Demkov model, increase with increasing projectile energy. This is due to the fact that the transitions are produced by dynamic coupling effects initiated by the nuclear-electron interaction, which require kinetic energy from the collision partners. In contrast, the cross section for dielectronic transitions leading to He$^+$ ($n=1$) formation decreases with increasing projectile energy. The dielectronic mechanism resembles the Auger effect caused by the electron-electron interaction and does not require kinetic energy from the collision partners. This becomes less important when the projectile energy increases and the collision time decreases.

V. CONCLUSIONS

We have made a comprehensive study of state selective single electron capture by He^{2+} ions over a wide energy range from 0.025–12 keV amu^{-1}. Nondissociative capture into the $n=2$ states of He$^+$ is the dominant channel for collision energies above 250 eV amu^{-1} while dissociative transfer ionization leading to He$^+$ ($n=1$) formation dominates at lower energies. Simple model calculations have been applied to satisfactorily explain this behavior. Capture into $n=3$ states of He$^+$ never accounts for more than a few percent of the total one-electron capture cross section. Our measured cross sections have also been shown to be in reasonable agreement with cross sections calculated using the Demkov and Landau-Zener models.

[1] T. E. Cravens, Science **296**, 1042 (2002).

[2] P. Beiersdorfer, C. M. Lisse, R. E. Olson, G. V. Brown, and H. Chen, Astrophys. J. Lett. **554**, L99 (2001).

[3] V. Kharchenko, M. Rigazio, A. Dalgarno, and V. A. Krasnopolsky, Astrophys. J. Lett. **585**, L73 (2003).

[4] D. Bodewits, Z. Juhász, R. Hoekstra, and A. G. G. M. Tielens, Astrophys. J. Lett. **606**, L81 (2004).

[5] D. Bodewits, R. W. McCullough, A. G. G. M. Tielens, and R. Hoekstra, Phys. Scr. (to be published).

[6] M. E. Rudd, T. V. Goffe, and A. Itoh, Phys. Rev. A **32**, 2128 (1985).

[7] K. Ishii, K. Okuno, and N. Kobayashi, Phys. Scr. T **80B**, 176 (1999).

[8] J. B. Greenwood, A. Chutjian, and S. J. Smith, Astrophys. J. **529**, 605 (2000).

[9] J. B. Greenwood, R. S. Mawhorter, I. Čadež, J. Lonzano, S. J. Smith, and A. Chutjian, Phys. Scr. **T110**, 358 (2004).

[10] O. Abu-Haija, E. Y. Kamber, and S. M. Ferguson, Nucl. Instrum. Methods Phys. Res. B **205**, 634 (2003).

[11] D. M. Kearns, R. W. McCullough, and H. B. Gilbody, J. Phys. B **35**, 4335 (2002).

[12] E. Y. Kamber, O. Abu-Haija, and S. M. Ferguson, Phys. Rev. A **65**, 062717 (2002).

[13] J. E. Reutt, L. S. Wang, Y. T. Lee, and D. Y. Shirley, J. Chem. Phys. **85**, 6928 (1986).

[14] P. J. Richardson, J. H. D. Eland, P. G. Fournier, and D. L. Cooper, J. Chem. Phys. **84**, 3189 (1986).

[15] S. Bashkin and J. O. Stoner, Jr., *Atomic Energy Levels and Grotrian Diagrams* (North-Holland, Amsterdam, 1986).

[16] G. Lubinski, Z. Juhász, R. Morgenstern, and R. Hoekstra, Phys. Rev. Lett. **86**, 616 (2001).

[17] R. Hoekstra, F. J. de Heer, and R. Morgenstern, J. Phys. B **24**, 4025 (1991).

[18] Z. D. Pešić, J-Y Chesnel, R. Hellhammer, B. Sulik, and N. Stolterfoht, J. Phys. B **37**, 1405 (2004).

[19] Y. N. Demkov, Zh. Eksp. Teor. Fiz. **45**, 195 (1963) [Sov. Phys. JETP **18**, 138 (1964)].

[20] C. D. Landau, J. Phys. (Moscow) 2, 46 (1932).

[21] C. Zener, Proc. R. Soc. London, Ser. A, **137**, 696 (1932).

[22] A. Salop and R. E. Olson, Phys. Rev. A **13**, 1312 (1976).

[23] N. Stolterfoht, *Progress in Atomic Spectroscopy Part D*, edited by H. Kleinoppen (Plenum Press, New York, 1987), p. 415.

[24] N. Stolterfoht, Phys. Rev. A **47**, R763 (1993).